Chemotactic movement of a polarity site enables yeast cells to find their mates

Debraj Ghose[a,b,1], Katherine Jacobs[b,1], Samuel Ramirez[c], Timothy Elston[c], and Daniel Lew[b,2]

[a]Computational Biology and Bioinformatics, Duke University, Durham, NC 27710; [b]Department of Pharmacology and Cancer Biology, Duke University Medical Center, Durham, NC 27710; and [c]Department of Pharmacology, University of North Carolina at Chapel Hill, Chapel Hill, NC 27599

Edited by Jasper Rine, University of California, Berkeley, CA, and approved April 27, 2021 (received for review December 10, 2020)

How small eukaryotic cells can interpret dynamic, noisy, and spatially complex chemical gradients to orient growth or movement is poorly understood. We address this question using *Saccharomyces cerevisiae*, where cells orient polarity up pheromone gradients during mating. Initial orientation is often incorrect, but polarity sites then move around the cortex in a search for partners. We find that this movement is biased by local pheromone gradients across the polarity site: that is, movement of the polarity site is chemotactic. A bottom-up computational model recapitulates this biased movement. The model reveals how even though pheromone-bound receptors do not mimic the shape of external pheromone gradients, nonlinear and stochastic effects combine to generate effective gradient tracking. This mechanism for gradient tracking may be applicable to any cell that searches for a target in a complex chemical landscape.

cell polarity | chemotropism | modeling | yeast | pheromone

Many cells—including neutrophils, *Dictyostelium* amoebae, cancer cells, neurons, and yeast—move or grow in a direction influenced by chemical gradients (1–4). These cells use G protein-coupled receptors (GPCRs) to sense external signals and regulate cytoskeletal components to direct movement or growth (5). How cells convert an external chemical gradient into a directed response remains poorly understood. We address this question for the genetically tractable budding yeast, *Saccharomyces cerevisiae*.

Haploid yeast of mating types **a** and α mate to form zygotes. **a** and α cells express specific GPCRs that sense pheromones secreted by the opposite mating type. Pheromone binding triggers GDP/GTP exchange on Gα, freeing G$\beta\gamma$ to activate downstream pathways. G$\beta\gamma$ recruits the scaffold protein Ste5 from the cytoplasm to the membrane, activating a MAPK cascade that results in expression of mating-specific genes, cell-cycle arrest in G1 phase, and polarization of Cdc42 (Fig. 1*A*) (6).

Mating requires polarized secretion to remodel the cell wall at the contact site between partner cells. Polarity is initiated and maintained by the conserved Rho-family GTPase Cdc42, which cycles between active GTP-Cdc42 and inactive GDP-Cdc42. Activation and inactivation are catalyzed by guanine exchange factors (GEFs) and GTPase activating proteins (GAPs), respectively (7, 8). GTP-Cdc42 at the plasma membrane recruits a GEF from the cytoplasm that locally activates nearby GDP-Cdc42, raising the local GTP-Cdc42 concentration to make a polarity patch (9–12). After polarity patch formation, Cdc42 orients actin cables toward the patch, delivering secretory vesicles that promote remodeling of the cell wall (13–15).

How does a cell orient its polarity patch toward the partner? Recent work indicates that many, and perhaps most, mating yeast cells initially polarize in the wrong direction (16, 17). Subsequently, polarity patches move and dissolve/reform in an erratic manner during an indecisive phase before strengthening and stabilizing in the correct orientation (16, 18, 19). Patch movement has also been observed in artificial pheromone gradients (20–23) and even in cells with genetically activated MAPK that were not exposed to pheromone at all (24, 25). Patch movement is thought to represent a search process that serves to improve orientation (26, 27).

Due to polarized secretion and endocytosis, GPCRs and associated G proteins become enriched at the membrane surrounding the polarity patch, generating a sensitized region for pheromone sensing (24, 28–33). The polarity patch also acts as a pheromone emission site, because pheromones and pheromone transporters are delivered by secretory vesicles (18, 34). This means that each moving patch is both a signal-emitting hub ("here I am!") and a sensing hub ("is anyone there?"), suggesting that yeast cells find their mates by "exploratory polarization" (Fig. 1*B*). In this model, adjacent cells of opposite mating type whose patches are not aligned sense low levels of pheromone because pheromone released from one patch dissipates rapidly with distance (Fig. 1 *B*, *ii*). As the patches move around the cortex (Fig. 1 *B*, *iii*), they may align (Fig. 1 *B*, *iv*), so that each patch detects a large increase in pheromone concentration and stalls their movement (Fig. 1 *B*, *iv*).

When cells are exposed to high pheromone levels, patch movement is stalled (20, 24). This reduction is due to a signaling pathway in which free G$\beta\gamma$ near pheromone-bound GPCRs recruits the scaffold protein Far1, which binds to the Cdc42-directed GEF (24, 35–37). These observations suggest that yeast polarity sites may search for each other by wandering randomly until they happen to align, at which point both cells detect high pheromone levels and the G$\beta\gamma$-Far1-GEF pathway stops patch movement. This model is conceptually very similar to the "speed dating" model proposed for the fission yeast *Schizosaccharomyces pombe* (38). Alternatively, it could be that the movement of the polarity site during the initial search phase is guided toward the partner by a pheromone gradient. Here we find that polarity patches of mating cells find each other much more rapidly than can be accounted for by an undirected

Significance

Many cells use extracellular chemical gradients to orient growth or movement in a specific direction. This is critical for development, wound healing, innate immunity, axon guidance, fertilization, and many other processes. However, how cells convert a chemical gradient into a directional response is poorly understood. We use the budding yeast as a model system for gradient sensing and combine experiments and computational modeling to propose a mechanism for how a cell can decode complex and dynamic spatial chemical gradients. The mechanism involves exploration by a subcellular front and may yield clues to other search processes where cells extend projections to seek out specific targets.

Author contributions: D.G., K.J., and D.L. designed research; D.G. and K.J. performed research; D.G., K.J., S.R., T.E., and D.L. analyzed data; T.E. and D.L. secured funding for research; and D.G., K.J., S.R., T.E., and D.L. wrote the paper.

The authors declare no competing interest.

This article is a PNAS Direct Submission.

[1]D.G. and K.J. contributed equally to this work.

[2]To whom correspondence may be addressed. Email: daniel.lew@duke.edu.

This article contains supporting information online at https://www.pnas.org/lookup/suppl/doi:10.1073/pnas.2025445118/-/DCSupplemental.

Published May 28, 2021.

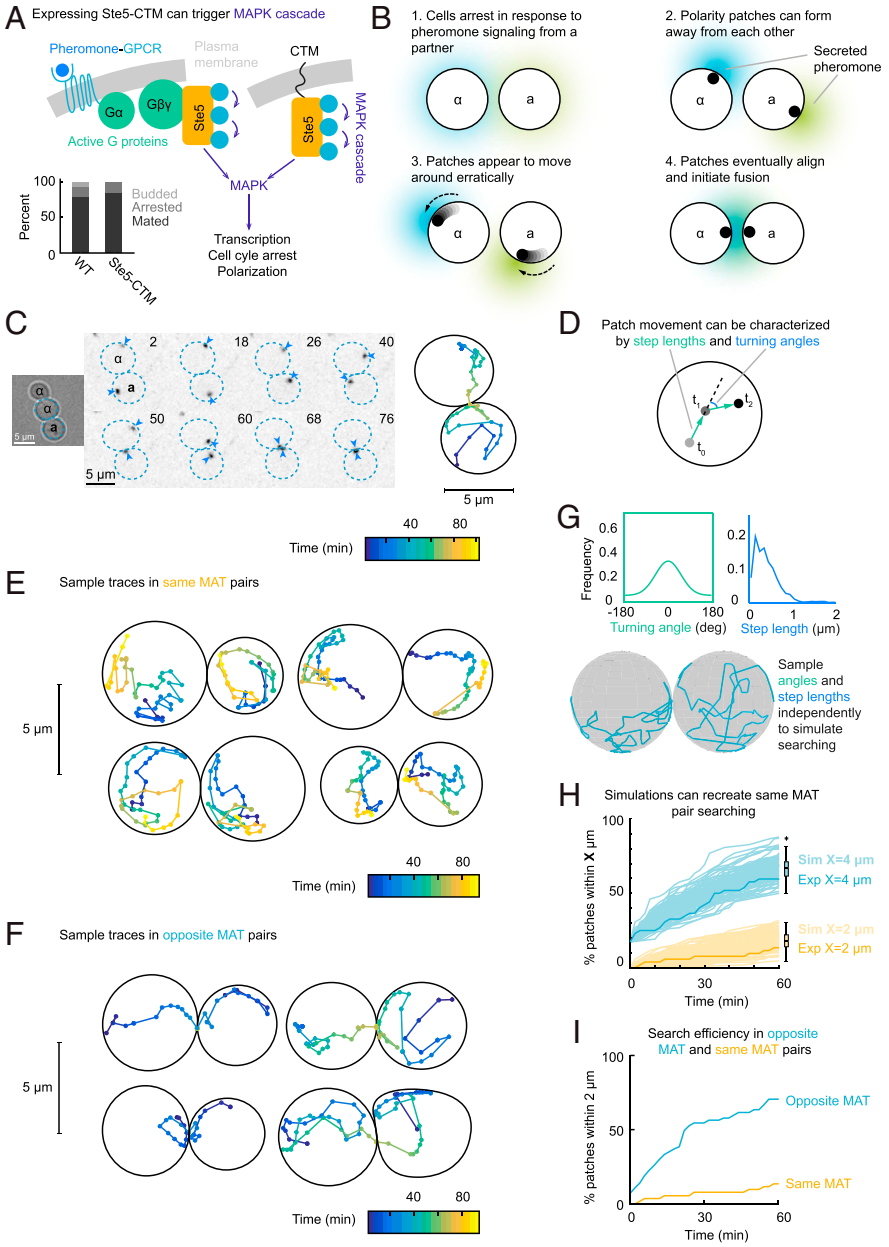

Fig. 1. Polarity patch movement is influenced by the mating partner. (*A*) Pheromone–receptor binding triggers release of Gβγ, which recruits the scaffold protein Ste5 to the membrane and activates MAPK signaling. An artificially membrane-targeted Ste5-CTM activates MAPK signaling in the absence of pheromone. (*Bottom Left*) Mating efficiency (*Materials and Methods*) of wild-type (WT) and Ste5-CTM cells. $n = 113$ cells for each condition. (*B*) Exploratory polarization. Colors represent a-factor (green) and α-factor (blue) pheromones. (*i*) Cells of opposite mating type (MAT) prior to polarization. (*ii*) Cells initially polarize in the wrong direction and secrete pheromones away from each other. (*iii*) Sensing low pheromone levels, polarity patches move along the cortex. (*iv*) When polarity patches align, they sense high pheromone levels and stop moving. (*C*) Polarity patch movement in a mating pair. Cells (DLY20626 and DLY20627) were treated with β-estradiol for 3 h to induce Ste5-CTM and then imaged. Inverted maximum projection images show Spa2 patches (blue arrowheads). Dotted blue lines outline the cells. Time is in min. (Scale bar, 5 μm.) (*Right*) The Spa2 centroid trajectory (projected from 3D to 2D). (*D*) Patch trajectory analysis: each 2-min time step yields a step length and turning angle. (*E* and *F*) Patch trajectories in pairs of cells (DLY20626, DLY20627) treated and analyzed as in *C*. Each pair consists of cells of the same MAT (*E*) or cells of opposite MAT (*F*). (*G*) Simulated patch trajectories were generated by sampling from the experimental distributions of step lengths and turning angles (graphs). A single example is shown. (*H*) Cumulative distribution of the time it took for patches to come within 4 or 2 μm of each other for populations of simulated cells (faint lines, Sim; 100 simulations of 52 pairs per condition) compared to same-sex yeast cells (dark lines, Exp). Box and whisker plots indicate median, quartiles, and 95th percentiles for simulated data. (*I*) Cumulative distribution of the time it took for patches to come within 2 μm of each other for opposite MAT (blue, $n = 57$) and same MAT (yellow, $n = 52$) pairs. Two-sample KS test, $P = 4\times10^{-11}$.

search and show that the direction of patch movement is biased toward the partner's patch.

A mechanistic computational model that incorporates Cdc42 biochemistry (11, 39, 40) and vesicle trafficking (20, 41–43) can quantitatively reproduce polarity patch movement characteristics in the absence of pheromone (25). We show that addition of a pheromone signaling pathway (24) causes this model to exhibit biased patch movement up pheromone gradients. Analysis of the

model suggests a mechanism whereby cells can effectively bias patch movement despite highly variable GPCR distributions on the cell cortex.

Results

Tracking Polarity Patches during the Search for a Mating Partner. The simplest version of exploratory polarization is one where the polarity patches of adjacent partners move randomly around the cell cortex until they find each other. While polarity patches during the indecisive stage are too fleeting to track accurately (16), artificial MAPK activation by expression of membrane-targeted Ste5 (Ste5-CTM, a gain-of-function condition) arrests cells in G1 (Fig. 1*A*) and strengthens polarity (24), allowing us to track polarity patches. In these cells, as in cells treated with high pheromone levels, polarity patches form at sites designated by bud-site-selection cues interpreted by the GTPase Rsr1 (22, 44). Upon deletion of *RSR1*, the polarity patch wanders around the cortex even in the absence of pheromone, and its movement can be readily tracked (24, 25). Mating efficiency is comparable in wild-type cells and cells induced to express Ste5-CTM (Fig. 1 *A*, *Inset*). Tracking patch centroids in three dimensions (3D) generates movement trajectories that can be decomposed into a series of steps. Each step is characterized by its magnitude (step length) and direction with respect to the preceding step (turning angle) (Fig. 1*D*). This system allows us to track polarity patch movement during the partner search that culminates in mating.

Cells of opposite mating type (MAT) with a fluorescent polarisome component Spa2 (45) were separately induced to express Ste5-CTM. The mating types were mixed together on agarose slabs and imaged. Isolated cell pairs were selected for analysis, such that each cell had only one potential (touching) mating partner (Fig. 1*C* and Movies S1 and S2). Adjacent pairs of opposite mating type can communicate via pheromones, while pairs of the same mating type cannot. Thus, comparison of patch movement in same-sex and opposite-sex pairs reveals the effects of pheromone-mediated communication.

Example centroid trajectories are shown in Fig. 1 *E* and *F* (Movies S1 and S2). To measure search efficiency, we recorded the cumulative fraction of cells whose patches got within some distance of each other over time. The patch's movement along the cell cortex could be recreated by simulating random movement on a sphere, sampling from experimentally obtained distributions of step lengths and turning angles (Fig. 1*G*; Bootstrapped statistics in *SI Appendix*, Fig. S1) (*Materials and Methods*) (25). Simulations displayed a similar search efficiency as same-sex pairs (Fig. 1*H*), supporting the assumption that same-sex cells do not communicate with each other. In contrast, opposite-sex pairs displayed a much higher search efficiency (Fig. 1*I*), implying that patches do not simply move randomly until they happen to find each other. Instead, signaling between opposite-sex cells greatly improves search efficiency.

Pheromone Gradients Bias the Direction of Patch Movement. We considered two potential mechanisms by which signaling might improve search efficiency. The first is based on the observation that patch movement decreases as the pheromone concentration increases (24). As sensing is primarily confined to a zone around the polarity patch, we imagine that in a pheromone gradient, the patch might move more on the down-gradient side (sensing less pheromone) than on the up-gradient side (sensing more pheromone) (Fig. 2*A*). Alternatively, the direction of patch movement might be biased by the pheromone gradient, so that a patch is more likely to move up-gradient than down-gradient (Fig. 2*A*). Regulation of the amount or the direction of patch movement would improve search efficiency, and the two mechanisms are not mutually exclusive.

To ask if the amount of patch movement varies as a function of the distance between the partners' patches, we combined the movies for 57 pairs of opposite-sex cells and plotted the step lengths taken by each patch in 2 min as a function of the distance between the partner patches (interpatch distance) at the start of the 2-min interval (Fig. 2*B*). For patch centroids that were farther apart than about 1.2 μm, there was no correlation between the step length and the interpatch distance (Fig. 2*C*). However, when the patch centroids were very close to each other, movement stopped. We conclude that at physiological pheromone concentrations, patches only slow down significantly when they are very close to each other (within one patch diameter).

To ask if the direction of patch movement is biased by the partner cell's patch, we measured the direction of movement for each step relative to a vector pointing to its partner's patch (the optimal direction) (Fig. 2*B*) (see *Materials and Methods* and *SI Appendix*, Fig. S2, for details). For same-sex cells, the direction of movement was uniformly distributed with respect to the partner's patch, but for opposite-sex cells, smaller angles (movement oriented in the direction of the partner patch) were overrepresented (Fig. 2*D* and *SI Appendix*, Fig. S3). This difference was statistically significant (Kolmogorov–Smirnoff [KS] test, $P = 4 \times 10^{-12}$) but modest in magnitude. To assess whether the extent of bias might depend on the distance between the partner patches, we compared the angles for steps taken from starting points with small (<4 μm) or large (>4 μm) interpatch distances. When partner patches were far apart, they showed almost no bias in the direction of patch movement, while patches that were closer displayed a much larger bias than the whole population (Fig. 2*E* and *SI Appendix*, Fig. S3) (KS test, $P = 10^{-11}$). Plotting the average angle of movement as a function of the distance between partner patches supported the same conclusion (Fig. 2*F*). In this plot, random movement yields angles uniformly distributed between 0° and 180°, for an average angle of 90°, while movement biased toward the partner patch yields smaller average angles. We conclude that when partner patches are distant from each other, movement is random. However, when they approach within <4 μm of each other, their direction of movement becomes increasingly biased toward their partners' patch.

Effect of the Landmark Protein, Rsr1. Rsr1 can lower accuracy of shmoo orientation up pheromone gradients for cells in a microfluidics device (22), suggesting that Rsr1 might also impair mating. In cells that express Ste5-CTM, introduction of Rsr1 made the cells form lumpy shmoos (44) (Fig. 3*A*), but they still relocated their polarity patches (Fig. 3*B* and Movie S3) and mated with comparable timing to cells lacking Rsr1 (Fig. 3*C*).

To ask whether patch movement is biased toward a partner cell's patch in cells with Rsr1, we adjusted our strategy to allow efficient analysis of more cells per movie. We mixed **a** and α cells induced to express Ste5-CTM on an agarose slab infused with saturating levels of α-factor. The α-factor immobilizes the polarity patches in the **a** cells, converting them into stationary sources of pheromone toward which α cells can track. Observing how several α cells responded to a source patch substantially increased the data yield from each movie. We quantified patch movement in α cells that were adjacent to an **a** cell patch at the interface between the two cells (*Materials and Methods* and *SI Appendix*, Fig. S4). As with the *rsr1* mutants described above, we observed a clear bias in the α cell patch's movement toward the partner patch (Fig. 3*D* and *SI Appendix*, Fig. S3) (KS test, $P = 7 \times 10^{-5}$). Thus, Rsr1 does not prevent cells from biasing the direction of patch movement.

G$\beta\gamma$-Far1-GEF Pathway Biases Patch Movement. Our findings indicate that the pheromone emitted by one cell biases the direction of patch movement in its partner. An obvious potential mechanism by which this could occur is via the Gβγ-Far1-GEF pathway. Previous studies identified a point mutation in the GEF Cdc24, *cdc24-m1*, that impairs Far1-GEF interaction but leaves other functions of both proteins intact (36, 46). In mutant cells, the mobile patch does not stop moving even in saturating pheromone (20, 24, 47), indicating that an intact Gβγ-Far1-GEF pathway is required to

CELL BIOLOGY

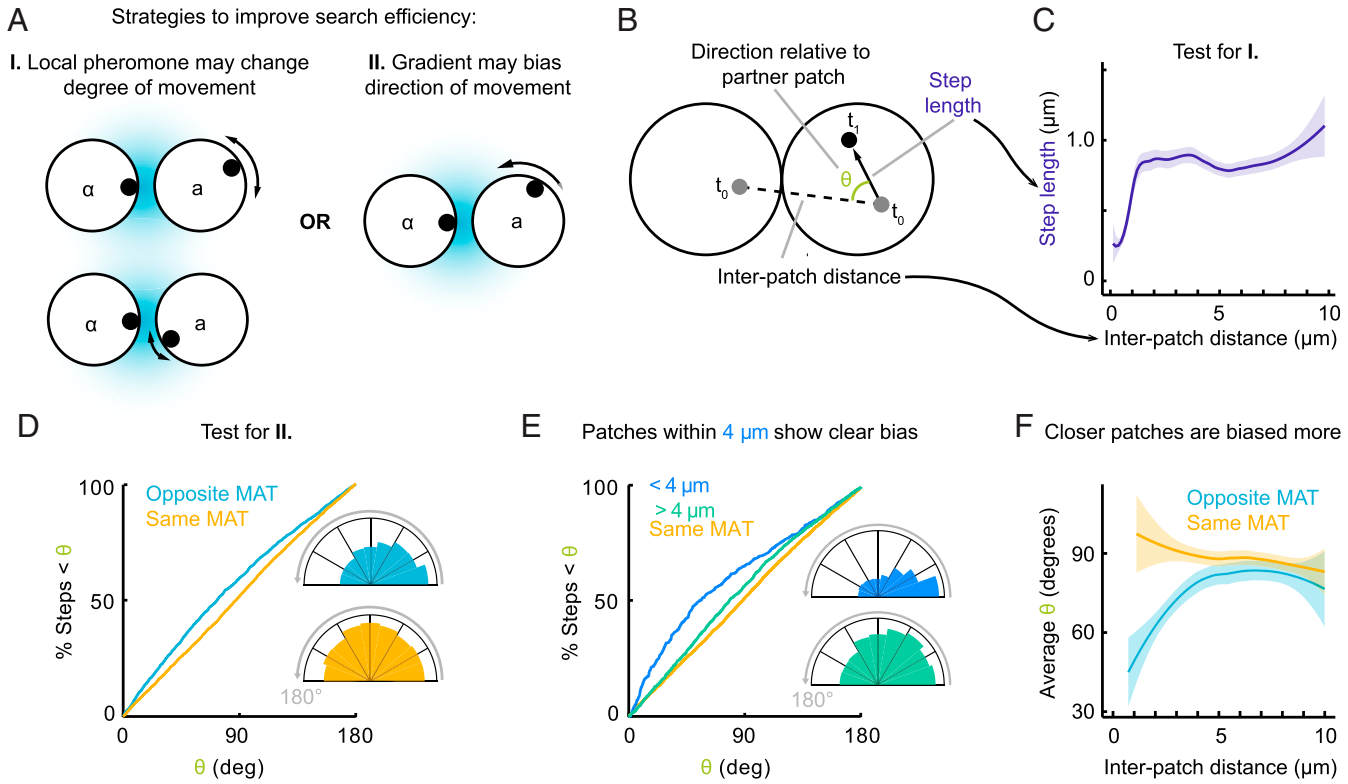

Fig. 2. The direction of polarity patch movement is biased by the pheromone gradient. (*A*) Potential mechanisms for accelerating patch alignment. (*I*) The amount of movement is biased by the pheromone gradient, with less movement at higher pheromone. (*II*) The direction of movement is biased by the pheromone gradient. (*B*) Patch trajectory measurements: step length (as in Fig. 1*D*), angle of patch movement (relative to an optimal vector toward its partner patch), and interpatch distance (between the two patches in a pair of cells). (*C*) Step length as a function of the interpatch distance for opposite MAT pairs (n = 1,497 steps). In order to track individual patches when they meet, we used strains with Spa2 probes in different colors. Mating mixtures are DLY20626 × DLY23007 or DLY20627 × DLY23008. Shading is 95% confidence interval. (*D*) Cumulative distribution of movement direction relative to the partner patch (θ) for steps from cells of opposite (blue, n = 2,289 steps) and same MAT (yellow, n = 4,501 steps). Two-sample KS test, $P = 4\times10^{-12}$. (*Inset*) Polar histograms of same data. (*E*) Cumulative distribution of θ for steps from opposite MAT pairs with interpatch distance <4 μm (blue, n = 594 steps) or >4 μm (green, n = 1,695 steps) Two-sample KS test, $P = 10^{-11}$. (*Inset*) Polar histograms of same data. (*F*) Average direction relative to the partner patch (*θ*) as a function of the interpatch distance for patches in opposite (blue, n = 2,289 steps) and same (yellow, n = 4,501 steps) MAT pairs. Shading is 95% confidence interval.

restrain patch movement. To ask whether the Gβγ-Far1-GEF pathway is also required to enable the directional bias of patch movement, we imaged opposite-sex pairs of *rsr1 cdc24-m1* mutants induced to express membrane-targeted Ste5. As anticipated, these cells did not mate, and the polarity patches continued to move (Fig. 3*E* and Movie S4). In addition, these mutants failed to show any directional bias toward the partner cells' patches (Fig. 3*F* and *SI Appendix*, Fig. S3), and the overall search efficiency was much closer to that of same-sex pairs than that of opposite-sex pairs with an intact Gβγ-Far1-GEF pathway (Fig. 3*G*). Thus, in addition to its documented role in halting patch movement, the Gβγ-Far1-GEF pathway serves to bias the direction of patch movement.

A Computational Model for Patch Movement in a Pheromone Gradient. The small size of the yeast cell makes it difficult for it to extract directional information by comparing pheromone concentrations across only a 4- to 5-μm distance (48–50). That an even smaller (<2 μm diameter) polarity patch should be able to bias its direction of movement in response to a pheromone gradient therefore seems remarkable. To understand how this occurs, we turned to a mechanistic computational model of patch movement (25), to which we added a computational representation of the Gβγ-Far1-GEF pathway based on (24). Previous work had shown that such a model could exhibit reduced patch movement in the presence of high levels of pheromone (24), and we wondered whether it would also exhibit a bias in the direction of patch movement in response to an applied pheromone gradient. If so, we hoped that in silico analyses would allow us to discriminate which mechanism would best enable a polarity patch to track a gradient and suggest how such a small patch could effectively respond to the gradient.

We begin by providing a brief description of the model; details are provided in *SI Appendix*. The model considers polarity protein biochemical reactions and actin-mediated vesicle traffic (25). Reaction–diffusion equations simulate patch formation through a positive feedback loop that promotes local GTP-Cdc42 accumulation (11, 39) (*SI Appendix*, Fig. S5*A*). This polarity module produces a stable patch that is in dynamic equilibrium, balancing diffusion of proteins with rapid protein exchange between the plasma membrane and cytosol. Patch movement occurs upon addition of the vesicle trafficking module, where GTP-Cdc42 directs stochastic actin-mediated vesicle delivery to the patch (41–43). Vesicles perturb the patch by dilution and inactivation of GTP-Cdc42, which can displace the patch's centroid. On a timescale of minutes, vesicle-induced asymmetric gain and loss of Cdc42 from opposite sides of the patch causes movement of the patch centroid (*SI Appendix*, Fig. S5*B*). As expected from this mechanism, imaging of both a polarity marker (Bem1-GFP) and a polarisome component (Spa2-mCherry) that marks the sites of vesicle exocytosis (24) showed polarity site movement away from the sites of vesicle accumulation (*SI Appendix*, Fig. S5*B*, *Bottom Inset*).

In addition to exocytosis, the vesicle trafficking module includes stochastic endocytosis events, which allow for removal or

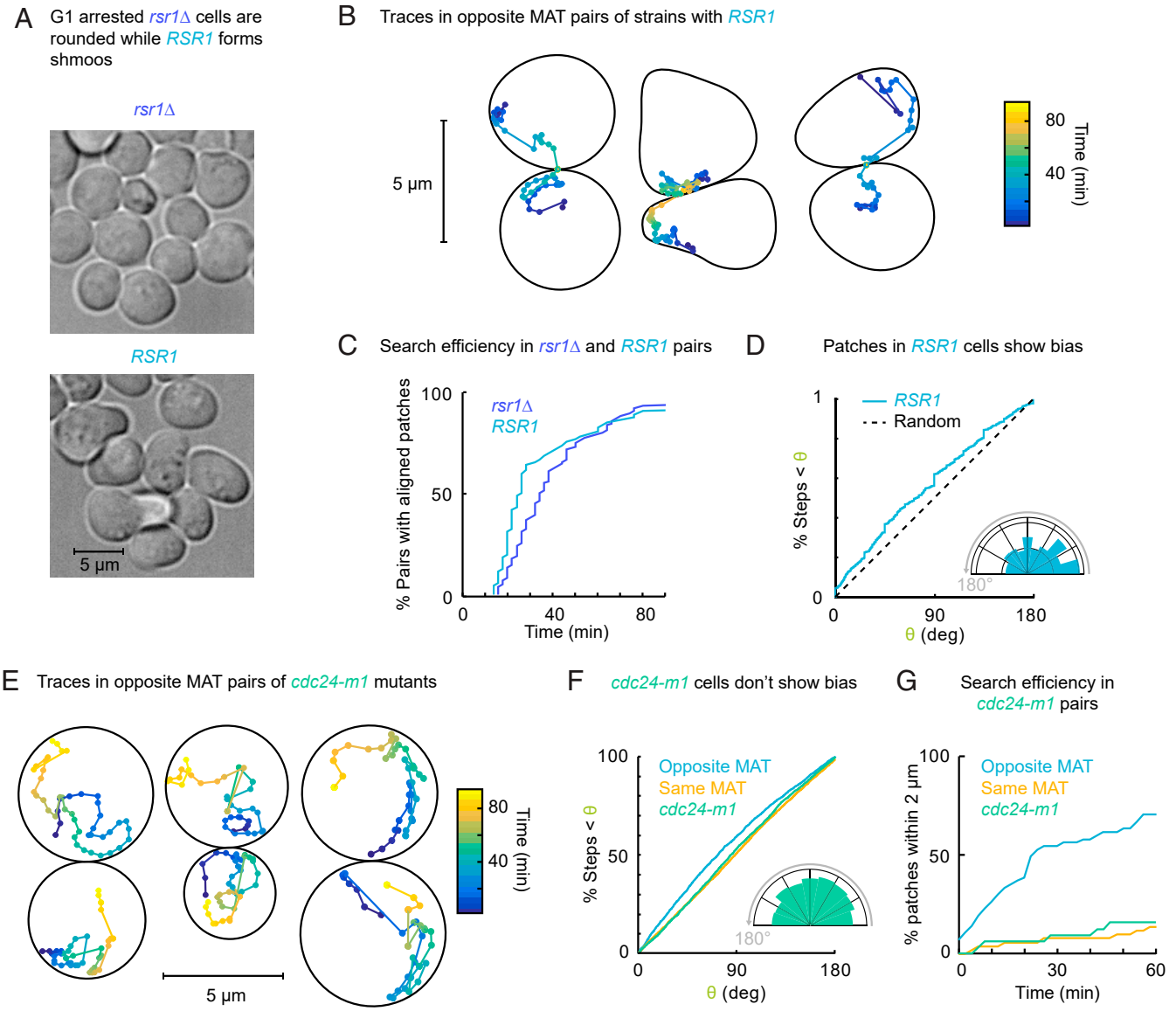

Fig. 3. Effect of Rsr1 and Gβγ-Far1-GEF pathway. (*A*) DIC images of *rsr1*Δ (DLY20626 × DLY20627) and *RSR1* (DLY21957 × DLY21958) mixes after pretreatment with β-estradiol for 3 h. (*B*) Polarity patch movement in opposite MAT *RSR1* pairs. Cells (DLY21957 and DLY21958) were treated with β-estradiol for 3 h to induce Ste5-CTM, mixed, and imaged. Spa2 centroid trajectories projected from 3D to 2D. (*C*) Cumulative distribution of the time it took patches to become aligned with the patch of the partner for *rsr1*Δ ($n = 85$) and *RSR1* ($n = 73$) opposite MAT pairs. Two-sample KS test, $P = 0.003$. (*D*) The cumulative distribution of movement direction relative to the partner patch (θ) for steps from cells with *RSR1* (DLY22602) toward a pheromone source (DLY18172) ($n = 681$ steps). Dashed line indicates uniform distribution of angles. KS test, $P = 7\times10^{-5}$. (*Inset*) Polar histogram of same data. (*E*) Mating mixes of *rsr1*Δ *cdc24-m1* (DLY22532 and DLY22533) cells were treated and analyzed as in *B*. (*F*) The cumulative distribution of the direction relative to the partner patch (θ) for steps from *CDC24* (blue, $n = 2{,}289$ steps) or *cdc24-m1* (green, $n = 2{,}352$ steps) opposite MAT pairs and *CDC24* same MAT pairs (yellow, $n = 4{,}501$ steps). Opposite MAT *cdc24-m1* v. *CDC24*: two-sample KS test, $P = 9\times10^{-8}$. *cdc24-m1* vs. same MAT, not significant. (*Inset*) Polar histogram of *cdc24-m1* data. (*G*) The cumulative distribution of the time it took patches to come within 2 μm of each other for opposite MAT (blue, $n = 57$), same MAT (yellow, $n = 52$), and *cdc24-m1* opposite MAT (green, $n = 32$) pairs. Opposite MAT *cdc24-m1* vs. *CDC24*, two-sample KS test, $P = 4\times10^{-8}$. *cdc24-m1* vs. same MAT, not significant.

recycling of membrane proteins to an internal membrane compartment. Combining these processes leads to a Cdc42 concentration profile whose dynamics quantitatively mimic the undirected movement of a polarity patch that occurs in the absence of pheromone (*Materials and Methods*) (25).

To make the model responsive to pheromone, we introduced a simplified Gβγ-Far1-GEF pathway (24). In cells, GPCR activation releases Gβγ, which recruits Far1-GEF complexes from the cytoplasm to the membrane in the vicinity of active GPCR. Thus, pheromone binding results in local activation of Cdc42, which can then recruit more Cdc42 by positive feedback. This pathway is modeled through a species in the model called *Rec*, which represents the GPCR. *Rec* is delivered to the plasma membrane on exocytic vesicles. There it can bind to extracellular pheromone, making it susceptible to endocytic internalization and degradation. Pheromone-bound *Rec* (now called *RecGEF*) is endowed with GEF activity (*SI Appendix*, Fig. S5*C*). This assumes that the GEF recruited by the Gβγ-Far1-GEF pathway remains localized to sites with pheromone-bound GPCRs (or, equivalently, that active Gβγ does not diffuse far from its site of release before rebinding Gα).

Several parameters of the Gβγ-Far1-GEF pathway are well constrained by experimental data (*Materials and Methods*). However,

the amount of Cdc42 activation induced by this pathway is unknown and constitutes a free parameter in the model. Variation of this parameter revealed three broad regimes of model behavior, depending on whether the amount of GEF recruited by the Gβγ-Far1-GEF pathway is small, similar, or large compared to that in the polarity module. When it is small, the pathway has little effect on polarity patch behavior. When it is large, the polarity patch dissolves, and the active Cdc42 profile simply follows the *RecGEF* profile arising from stochastic vesicle traffic and pheromone binding. Neither of these regimes seems applicable to cell behavior, so we chose values of the free parameter that make the amount of GEF recruited by the Gβγ-Far1-GEF pathway comparable to that in the polarity module. In this regime, a polarity patch persists, but its behavior is influenced by pheromone.

Previously, a differently parameterized version of this model was used to show that high levels of spatially uniform pheromone could slow or stop polarity patch movement (24). This was interpreted as follows: 1) the vesicle delivery that perturbs Cdc42 at the polarity patch also inserts new GPCRs; 2) upon binding pheromone, these GPCRs activate Cdc42; and 3) GPCR-induced Cdc42 activation counteracts the initial Cdc42 perturbation, returning the patch centroid toward its previous position (*SI Appendix*, Fig. S5*D*). We first confirmed that our model also shows reduced patch movement with increasing pheromone (*SI Appendix*, Fig. S5 *E* and *F* and Movie S5). Patch movement displayed some persistence (i.e., a tendency to keep moving in the same direction, which makes turning angles smaller) on a 1-min timescale, and persistence was higher in the absence of pheromone than with spatially uniform pheromone (*SI Appendix*, Fig. S5*G*). On a longer 5-min timescale, patch movement in the absence of pheromone appeared more random/less persistent (*SI Appendix*, Fig. S5*G*). In the presence of pheromone, the patch movement became antipersistent (i.e., displayed a tendency to reverse direction and return to its previous position). A quantification of persistence confirmed that the patch had lower persistence or antipersistence when exposed to pheromone (*SI Appendix*, Fig. S5*H*). These results suggest that a patch navigating a spatially varying pheromone landscape would move persistently when it detects low pheromone levels but tend to wiggle in place when it detects higher pheromone levels.

The Direction of Patch Movement in the Model Is Biased up Pheromone Gradients. To ask how pheromone gradients would impact polarity patch behavior, we exposed the model to linear gradients of pheromone and tracked the centroid of active Cdc42 over 45 min (Fig. 4 *A*–*C* and *SI Appendix*, Fig. S6). As expected, there was no bias in patch movement orthogonal to the gradient (Fig. 4*D*). However, averaging of around 400 simulations revealed a clear bias of movement up the gradient, with greater bias up steeper gradients (Fig. 4*E*). Most simulated patches showed net movement up-gradient (Fig. 4*F*). Thus, a mechanistic model based on observations of patch behavior in uniform pheromone is capable of tracking spatial gradients of pheromone.

How does the model track the pheromone gradient? The computational patch moves less at higher levels of pheromone (*SI Appendix*, Fig. S5), which could yield less movement on the up-gradient side of a pheromone gradient (as in Fig. 2 *A*, *Left*). Alternatively, the pheromone gradient could bias direction of patch movement (as in Fig. 2 *A*, *Right*). These possibilities are not mutually exclusive, and it seemed possible that both might contribute to gradient tracking. To tease apart the contributions of changing amount of movement vs. biased directionality, we generated computational scenarios in which only one mechanism at a time could be operative.

The key to tracking due to variable movement is that when the patch happens to move up-gradient, it detects a higher level of pheromone and hence moves less. This mechanism does not require any difference in the pheromone concentration across the patch: the entire patch only needs to experience different pheromone levels in different parts of the gradient. In contrast, the key to a biased directionality is that there is a difference in the pheromone concentration from one side of the patch to the other. It is not necessary, for this mechanism, that there be any difference in average pheromone level when the patch visits different locations.

In the simulations of Fig. 4 *A*–*F*, there was both a position-dependent difference in average pheromone and a gradient of pheromone across the patch. However, by applying the gradient in different ways, we generated scenarios where there is only one (Fig. 4 *G*–*I*) or the other (Fig. 4 *J*–*L*). To expose the patch to a position-dependent difference in average pheromone without a gradient, we simulated the patch in uniform pheromone but made the pheromone concentration change as a function of the patch position (Fig. 4*G* and Movie S5). To expose the patch to a pheromone gradient without any location-dependent difference in average pheromone level, we generated a pheromone gradient that moved with the patch's centroid, so that the patch was always at the center of the gradient (Fig. 4*J*).

When patches were exposed to only a position-dependent difference in average pheromone, the patch did not exhibit an obvious bias in its final position (Fig. 4 *H* and *I*; compare to Fig. 4 *D* and *F*). However, when patches were exposed to only a gradient of pheromone across the patch, there was a clear bias that was even greater than the bias in our original scenario (Fig. 4 *K* and *L*; compare to Fig. 4 *D* and *F*). This held true even in a 0- to 100-nM gradient, which exposes the patch to higher total pheromone (*SI Appendix*, Fig. S6). These findings suggest that a difference in pheromone concentration across the patch is necessary and sufficient for gradient tracking in the model. This outcome matches our experimental observations of directional bias in patch movement (Fig. 2).

Our findings also show that constrained movement of the patch by higher local mean pheromone levels is neither necessary nor sufficient for gradient tracking in the model. This is remarkable as the model was initially constructed based on the behavior of cells in uniform concentrations of pheromone (24), in anticipation that this effect (biased amount of movement) could enable gradient tracking. Instead, we found that this effect was undetectable for the gradients and simulation times we employed and that directional bias was much more effective. These findings raise the question of how the pheromone gradient can effectively impart directional bias on patch movement.

Directional Bias due to Asymmetric GEF Activity at the Periphery of the Polarity Patch. The simplest way to envisage how a directional bias is imparted to patch movement would be that the pheromone gradient is translated via GPCRs into a gradient of GEF activity for Cdc42. A difference in GEF activity across the patch would result in greater recruitment of polarity factors on the up-gradient side of the patch, displacing the patch centroid in that direction. In the model discussed above, a pheromone gradient is first converted into a spatially varying GEF activity that then affects patch movement. To directly analyze how an applied GEF profile would affect patch movement, we asked how a model containing only the polarity module of the model (without vesicle traffic or GPCRs) would respond to an applied gradient of GEF activity.

A linear gradient of GEF caused the centroid of the patch to move deterministically (if slowly) up the gradient (Fig. 5*A*). To better understand what part(s) of the GEF gradient contributed to patch movement, we exposed the model patch to spikes of GEF activity at different distances from the patch centroid (Fig. 5*B*). GEF activity at the patch periphery was most effective at causing centroid movement, while GEF activity at distant locations had no effect (Fig. 5*B*). Indeed, applying the same GEF gradient to only the periphery of the patch recapitulated the full patch movement inspired by the entire gradient, while applying the gradient

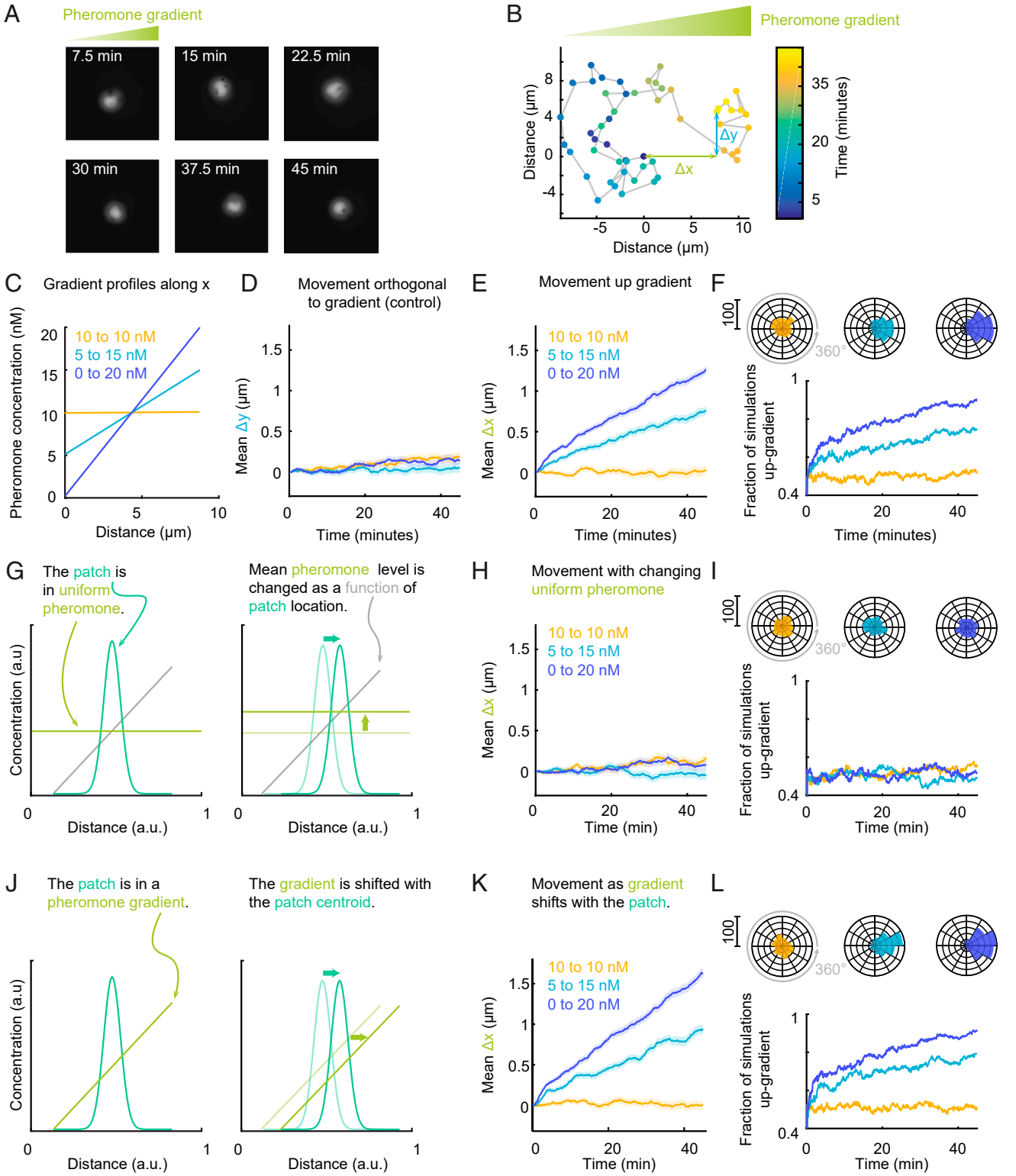

Fig. 4. Simulated polarity patch movement is biased by pheromone gradients. (*A*) Snapshots of simulated GTP-Cdc42 (*Cdc42T* + *BemGEF42*) concentration profile in a 0 to 20 nM pheromone gradient. (*B*) Example trace of patch centroid in 45 min simulation. The net displacement at 45 min along the *x* and *y* axis is shown. (*C*) Profiles of pheromone gradients presented to model. (*D*) Mean y displacement ($n = 380$ to 400 simulations) orthogonal to the gradient. Shading indicates SEM. (*E*) Mean × displacement ($n = 380$ to 400 simulations) in the direction of the gradient. (*F*) (*Top*) Polar plots showing distribution of 380 to 400 patch centroids at 45 min. (*Bottom*) Fraction of simulations with patch centroids up-gradient. (*G*) Simulation paradigm where the patch is exposed to uniform pheromone but pheromone levels change depending on the patch's location. a.u., arbitrary units. (*H* and *I*) Same as *E* and *F* but using simulation paradigm in *G*. (*J*) Simulation paradigm where the pheromone gradient moves with the patch centroid, so the mean pheromone is constant. (*K* and *L*) Same as *E* and *F* but using simulation paradigm in *J*.

everywhere else produced no movement (Fig. 5*C*). Thus, the impetus for patch movement derives primarily from asymmetric GEF activity at the periphery of the patch.

Localized negative feedback can counteract the tendency of positive feedback to reinforce the current patch position, making a peak more responsive to external cues (51). The destabilizing effect of vesicle traffic on the polarity peak can be considered as a localized negative feedback, in which case addition of vesicle traffic should potentiate patch movement in response to a GEF gradient. By promoting spontaneous patch movement, vesicle traffic introduced significant noise in the direction of movement, but in the presence of a GEF gradient, adding vesicle traffic enabled greater net movement in the up-gradient direction (Fig. 5*D*). We conclude that asymmetric GEF activity in the outskirts of the patch can bias patch movement, in a manner potentiated by vesicle traffic.

Gradient Tracking by the Full Model. The preceding analyses suggest that a GEF gradient across the patch (presumably caused by differential binding of pheromone to GPCRs at the patch periphery) could bias patch movement. However, translating an external pheromone gradient into an internal GEF gradient is not straightforward. GPCRs are distributed nonuniformly on the cell membrane, and the GEF distribution would depend not only on the pheromone gradient but also on the kinetics of GPCR secretion, GPCR endocytosis, and pheromone–GPCR binding/unbinding (*SI Appendix*, Fig. S7*A*).

To understand how an external pheromone gradient is translated into an internal GEF gradient, we visualized the spatial distribution of *RecGEF* (pheromone-bound GPCR with associated Gβγ-Far1-GEF) in simulations with a linear pheromone gradient. *RecGEF* distributions were quite variable but generally enriched in a broad zone reflecting where the polarity patch had delivered new GPCRs in the recent past (Fig. 6*A* and Movie S6). Averaging *RecGEF* profiles by aligning them by their centroids (*Materials and Methods*) revealed a peaked distribution (Fig. 6*B*). The asymmetry in *RecGEF* across the patch depends on the patch's location relative to the *RecGEF*'s centroid, which varied considerably (Fig. 6*C*). When a polarity patch made an excursion away from where it had recently deposited GPCRs, it often returned to the *RecGEF* zone (Fig. 6*D* and Movie S6). This antipersistent patch movement occurred on a 5-min timescale similar to that observed in uniform pheromone (*SI Appendix*, Fig. S5 *G* and *H*).

Antipersistent movement can be understood as follows: when a patch makes an excursion away from a zone where it had deposited *Rec*, the periphery of the patch is exposed to a steep GEF gradient because the patch is now located on the flank of the *RecGEF* peak (Fig. 6*E*). Histograms of *RecGEF* difference across the patch (Δ*RecGEF*, a measure of the GEF gradient) (Fig. 6 *F*, *Top Left*) (*Materials and Methods*) and patch movement (Fig. 6 *F*, *Top Right*) indicated that model patches experienced a broad range of GEF gradients both up- and down-gradient and also moved in both directions. Plotting the observed movement of the patch centroid as a function of Δ*RecGEF* revealed a strong correlation between patch movement (*y* axis) and Δ*RecGEF* experienced by the patch (*x* axis) (Fig. 6 *F*, *Bottom Left*), suggesting that *RecGEF* gradients motivate patch movement. In a gradient of pheromone, the patch experiences slightly more frequent and steeper GEF gradients in the direction of the pheromone gradient, leading to more frequent and greater movement of the patch in that direction (Fig. 6*F*). (Note increased frequency of points in the upper right quadrant, where positive GEF gradients drive movement up-gradient, for simulations in a pheromone gradient.) Thus, the patch moves, on average, up-gradient.

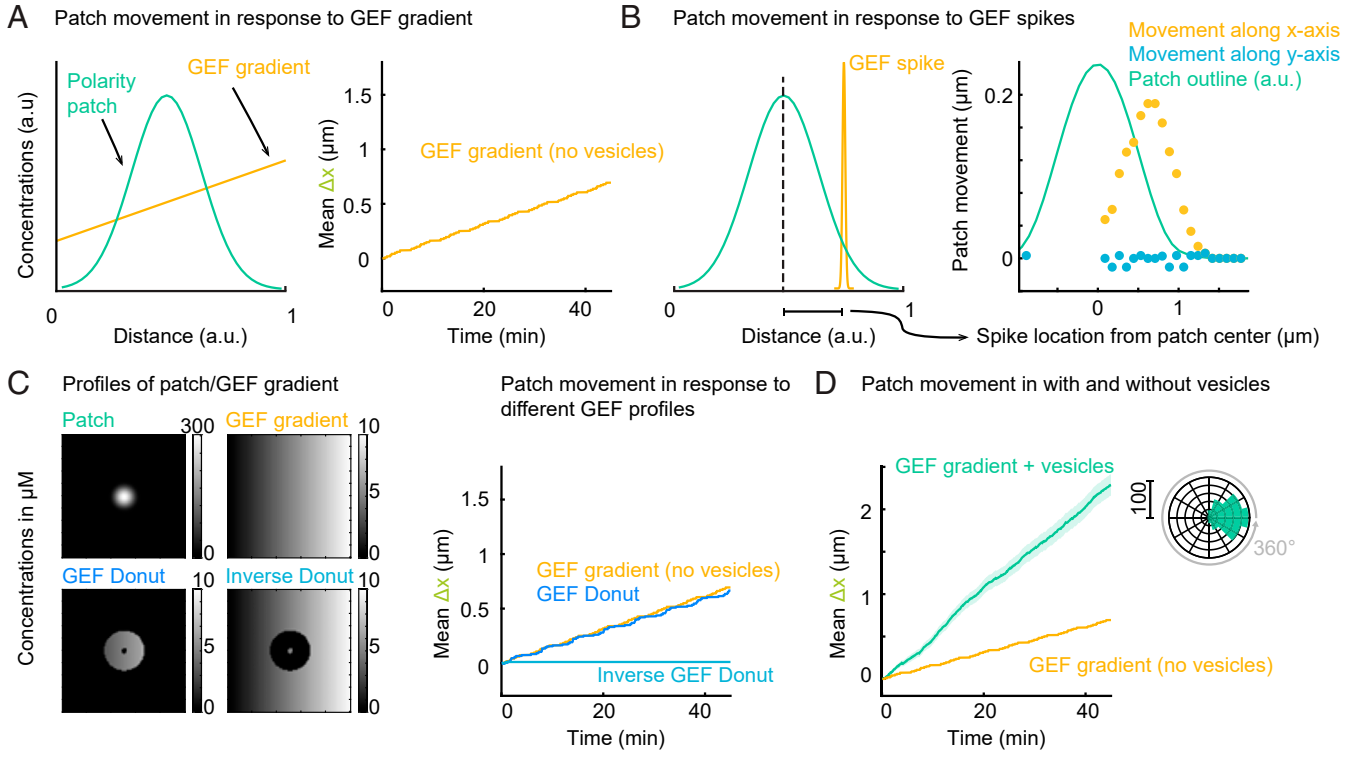

Fig. 5. Patch movement directed by a GEF gradient. (*A*) GEF activity gradient applied across a polarity patch (*Left*) causes gradual patch movement in the absence of vesicle traffic (*Right*). (*B*) Spikes of GEF activity (*Left*) cause patch movement (*Right*; 45 min simulation) whose amount depends on spike location. (*C*) (*Left*) Concentration profiles of GTP-Cdc42 patch (*Cdc42T* + *BemGEF*) and different GEF gradients. (*Right*) Patch movement depends only on GEF gradient at patch periphery (Donut). (*D*) Patch movement in response to GEF gradient is amplified by vesicle traffic. Shading indicates SEM for 400 simulations. (*Inset*) Polar histogram of patch centroids after 45 min.

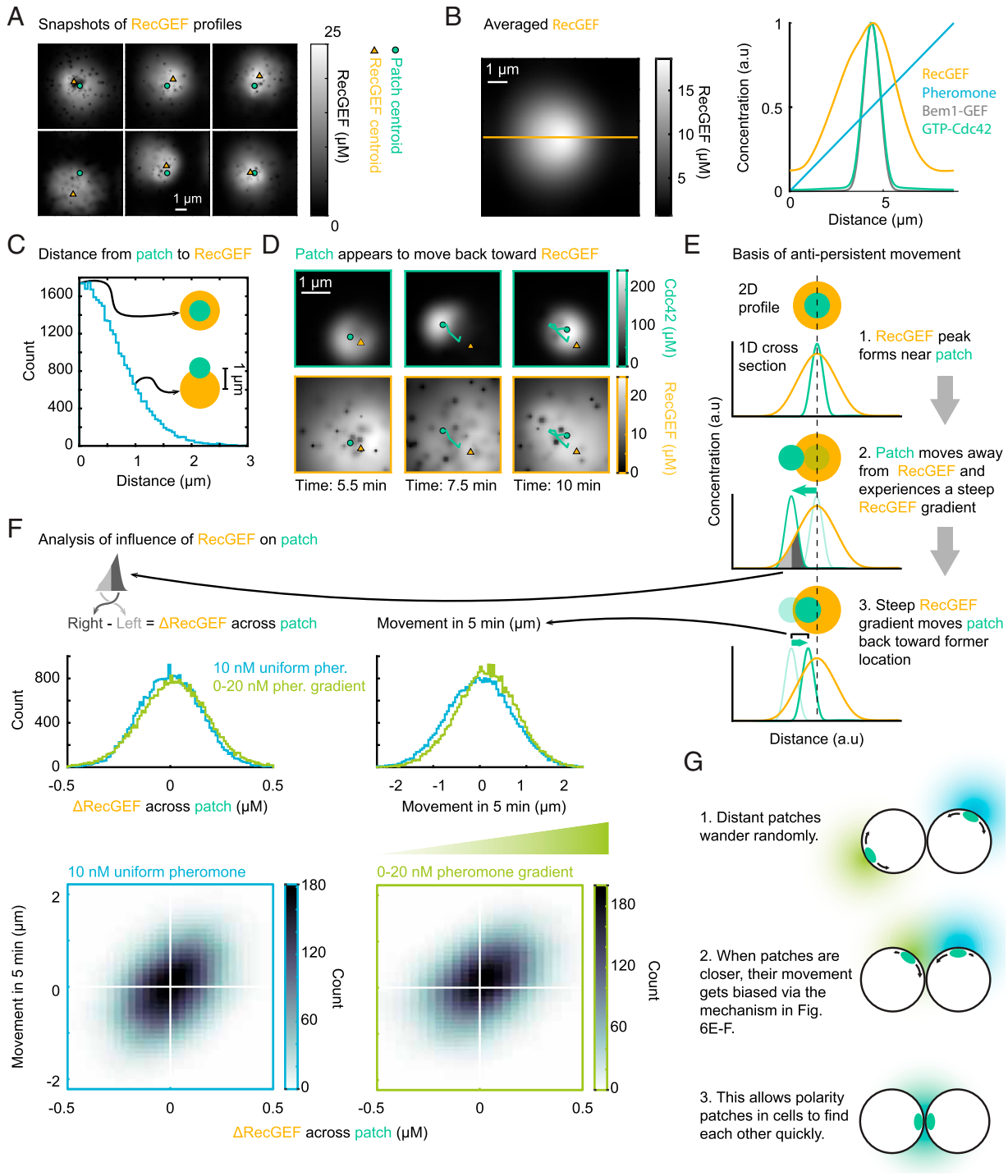

Fig. 6. Mechanism of gradient tracking by the model. (*A*) Snapshots of *RecGEF* (pheromone-bound GPCR) concentration. Dark dots indicate sites of endocytosis, green circle indicates GTP-Cdc42 (*Cdc42T* + *BemGEF42*) centroid, and yellow triangle indicates *RecGEF* centroid. (*B*) Averaged *RecGEF* distribution from 395 simulations in 0 to 20 nM pheromone gradient, shown in 2D (*Left*) and 1D cross section along with pheromone, average GTP-Cdc42, and average Bem1-GEF profiles (*Right*). Concentration normalized to maximum. (*C*) Histogram of distances between Cdc42 and RecGEF centroids. (*Insets*) Cartoons of patch and RecGEF distributions centered (*Upper*) or 1 μm apart (*Lower*). (*D*) Example of antipersistent patch movement: simulation showing Cdc42 (*Top*) and *RecGEF* (*Bottom*) distributions. (*E*) Cartoon of antipersistent movement mechanism. Concentration profiles of Cdc42 and *RecGEF* at different times. (*F*) (*Top*) Histograms of difference in *RecGEF* across the patch (Δ*RecGEF*; *Left*) and patch movement in 5 min (*Right*) in 10 nM uniform pheromone or 0 to 20 nM pheromone gradient. (*Bottom*) Scatterplots of patch movement vs. Δ*RecGEF*. Correlation between *RecGEF* gradient (*x* axis) and subsequent patch movement (*y* axis), plotted for 31,600 time points from 395 45-min simulations in 10 nM uniform pheromone (*Left*) and 0 to 20 nM pheromone gradient (*Right*). (*G*) Summary cartoon: patch movement is undirected when partner patches are distant, but as patches approach each other they experience steeper pheromone gradients that bias their movement toward each other until they meet.

As might be expected, changing the pheromone-GPCR binding parameters significantly altered the *RecGEF* profiles encountered by the polarity patch, but in all cases the linear pheromone gradient was translated into a peaked *RecGEF* profile that biased patch movement in the manner discussed above, so that gradient tracking was still effective (*SI Appendix*, Fig. S7).

Discussion

We show that yeast cells bias their polarity patch movement toward potential mating partners, and we propose a mechanistic basis for the bias. Because patch movement in wild-type cells is chaotic, with variable numbers of weak and transient polarity patches that are difficult to track, we used a strain in which membrane-tethered Ste5 induced MAPK activity, arresting cells in G1 with single clear polarity patches that allowed tracking using image analysis tools. Our findings suggest that a difference in pheromone concentration at the periphery of the patch can bias the direction of patch movement up-gradient. The observed bias is remarkable because the small size of the polarity patch (<2 μm in diameter) means the expected difference in pheromone concentration across that patch is minuscule. We argue that the unexpected efficacy of the directional bias stems from a combination of factors: 1) The pheromone gradient experienced by mating cells is steeper than previously appreciated because pheromones are secreted focally from the polarity site (18). 2) The external pheromone gradient is translated into an internal GEF landscape that includes GEF gradients much steeper than the pheromone gradient itself (*SI Appendix*, Fig. S7*D*). 3) The movement directed by steep local GEF gradients is amplified by vesicle traffic. These factors, discussed further below, combine to bias the directionality of polarity site movement, enabling rapid partner identification (Fig. 6*G*).

Pheromone Gradients Experienced by Mating Cells. Pheromone is emitted focally by secretion targeted to the polarity site, and theoretical considerations indicate that the pheromone gradient is much steeper closer to the emission site (18), thus providing a stronger directional signal. Consistent with these expectations, we found that partner sites within 4 μm of each other displayed directional bias toward each other, with the bias increasing as the sites got closer. At distances greater than 4 μm, the patches performed random search (25).

Elegant work on cells exposed to exogenous pheromone gradients in microfluidic devices demonstrated that bud-site-selection cues interpreted by Rsr1 could compete with the pheromone gradient to orient polarization, so that genetic removal of Rsr1 improved gradient tracking (22). In contrast, we found that the presence of Rsr1 did not impair or delay the partner search process in mating cells (Fig. 3*C*). We suggest that physiological pheromone gradients are much steeper than those in microfluidics devices and can outcompete Rsr1 to position the polarity site.

In the wild, cells might be surrounded by multiple potential mating partners (52, 53). The ability to engage with different partners, depending on which polarity sites are closest, provides a way to find single mating partners in a crowded environment.

Translating the External Pheromone Gradient into an Internal GEF Landscape. To guide the polarity site, the external pheromone gradient is translated into an internal GEF profile by GPCRs and the Gβγ-Far1-GEF pathway. The distribution of pheromone-induced GEF activity depends not only on the external pheromone concentration profile but also on the deposition of new receptors by the polarity site and the rates of pheromone–GPCR binding, unbinding, and endocytosis. These factors combine to distort a monotonic pheromone gradient into an uneven peaked distribution of GEF activity. As the polarity patch moves within this constantly evolving GEF landscape, it encounters local GEF gradients that are much steeper than the applied pheromone gradient. Steep GEF gradients bias Cdc42 activation to the up-gradient side of the patch, displacing the patch centroid in the direction of the gradient. While GEF gradients can occur in any direction, an external pheromone gradient preferentially steepens GEF gradients that align with the pheromone gradient, enabling gradient tracking.

Our computational model showed that the distribution of active GPCRs changed considerably when pheromone binding rate constants were varied over an order of magnitude (the reported range from experiments). Nevertheless, the ability of the polarity patch to track an applied pheromone gradient remained largely intact, attesting to the robustness of the mechanism outlined above.

Roles of Vesicle Traffic. In addition to its roles in sculpting the distribution of active GPCRs at the surface, our work highlights other important roles for vesicle traffic. One is the amplification of the patch movement brought about by GEF gradients (Fig. 5*D*). A second is to cause spontaneous polarity site movement even in the absence of a nearby partner (20, 24, 25), which allows the patch to explore the cortex and come within range of a partner's local pheromone gradient.

Roles of the Gβγ-Far1-GEF Pathway. Previous work indicated that the Gβγ-Far1-GEF pathway played two distinct roles: biasing the location at which a mating cell first assembles a polarity site (16) and stabilizing the polarity site so that it stops moving once it reaches a location where there is a high concentration of pheromone (24). Here we uncover a third role for this pathway, in biasing polarity site movement in response to pheromone gradients. Mutants that break the pathway by impairing Far1-GEF binding showed no bias in the direction of movement, so that it took much longer for adjacent cells' polarity sites to align. Thus, this single pathway connecting pheromone sensing to Cdc42 activation acts in three different ways to enable mating partners to locate each other.

Implications Beyond Budding Yeast. Prior work suggested that *S. pombe* sequentially assemble transient polarity patches at multiple locations (27, 38). When polarity patches from potential mating partners happen to coorient, the sites are stabilized (as they are in *S. cerevisiae*, though presumably by a different molecular mechanism because fission yeast lack the Gβγ-Far1-GEF pathway). A computational model assuming that polarity disassembly is prevented by exposure to high pheromone recapitulated cell–cell pairing of *S. pombe* on physiological timescales, without need for a mechanism to bias the location of polarity site formation (38). In contrast, our simulations of undirected polarity site movement in *S. cerevisiae* were unable to recapitulate the rapid timescale of partner alignment in budding yeast (Fig. 1 *G–I*). We note that this timescale is much faster in *S. cerevisiae* (minutes) than it is in *S. pombe* (hours). The exigencies of mating on a shorter timescale may have driven the evolution of an effective mechanism to guide the polarity site toward its partner in *S. cerevisiae*.

Although focused on mating in budding yeast, our findings have broad implications for any partner search process in which diffusible signals enable partners to locate each other in potentially crowded environments. In addition to other fungi (27, 54), aspects of the exploratory polarization strategy we discuss may apply to animal cells that develop cell type-specific local junctions with other cells. The best known such junctions (synapses) occur between neurons, or between neurons and various other cell types (55). However, similar specialized junctions develop in other contexts including between epithelial cells (56), between alveolar stem cells and fibroblasts in the lung (57), and between T cells and antigen-presenting cells (58). Development of such cell–cell contacts may involve cortical GTPase pathways like that of Cdc42, which direct cytoskeletal remodeling and vesicle trafficking to promote directional outgrowth of cell protrusions that meet to form junctions. It will be interesting to determine the extent to which

principles uncovered in yeast mating apply to partner search processes in other cells.

Materials and Methods

Yeast strains were generated using standard yeast genetics techniques and are listed in *SI Appendix*. Confocal time-lapse imaging was performed on spinning disk microscopes, and image analysis used custom scripts as described in *SI Appendix*. Computational modeling using MATLAB 2019b combined a reaction–diffusion model of polarity with stochastic vesicle traffic as described in *SI Appendix*.

Data Availability. Source code and experimental data have been deposited in GitHub (https://github.com/DebrajGhose/Chemotactic-polarity-site) (59). All other study data are included in the article and/or *SI Appendix*.

ACKNOWLEDGMENTS. We thank Stefano Di Talia, Masayuki Onishi, and members of the D.L. laboratory for reviewing the manuscript and/or stimulating discussions. We are also grateful to the Duke Light Microscopy Core Facility group (for assistance with operating confocal microscopes) and both Duke Compute Cluster and University of North Carolina at Chapel Hill Research Computing groups (for assistance with using computational resources). This work was funded by NIH/National Institute of General Medical Sciences grants R35GM127145 to T.E. and R01GM103870 and R35GM122488 to D.L.

1. E. T. Roussos, J. S. Condeelis, A. Patsialou, Chemotaxis in cancer. *Nat. Rev. Cancer* **11**, 573–587 (2011).
2. Y. Artemenko, T. J. Lampert, P. N. Devreotes, Moving towards a paradigm: Common mechanisms of chemotactic signaling in Dictyostelium and mammalian leukocytes. *Cell. Mol. Life Sci.* **71**, 3711–3747 (2014).
3. A. von Philipsborn, M. Bastmeyer, Mechanisms of gradient detection: A comparison of axon pathfinding with eukaryotic cell migration. *Int. Rev. Cytol.* **263**, 1–62 (2007).
4. R. A. Arkowitz, Chemical gradients and chemotropism in yeast. *Cold Spring Harb. Perspect. Biol.* **1**, a001958 (2009).
5. C. R. McCudden, M. D. Hains, R. J. Kimple, D. P. Siderovski, F. S. Willard, G-protein signaling: Back to the future. *Cell. Mol. Life Sci.* **62**, 551–577 (2005).
6. C. G. Alvaro, J. Thorner, Heterotrimeric G protein-coupled receptor signaling in yeast mating pheromone response. *J. Biol. Chem.* **291**, 7788–7795 (2016).
7. S. Etienne-Manneville, Cdc42—the centre of polarity. *J. Cell Sci.* **117**, 1291–1300 (2004).
8. H.-O. Park, E. Bi, Central roles of small GTPases in the development of cell polarity in yeast and beyond. *Microbiol. Mol. Biol. Rev.* **71**, 48–96 (2007).
9. J. G. Chiou, M. K. Balasubramanian, D. J. Lew, Cell polarity in yeast. *Annu. Rev. Cell Dev. Biol.* **33**, 77–101 (2017).
10. K. Witte, D. Strickland, M. Glotzer, Cell cycle entry triggers a switch between two modes of Cdc42 activation during yeast polarization. *eLife* **6**, e26722 (2017).
11. A. B. Goryachev, A. V. Pokhilko, Dynamics of Cdc42 network embodies a Turing-type mechanism of yeast cell polarity. *FEBS Lett.* **582**, 1437–1443 (2008).
12. B. Woods, D. J. Lew, Polarity establishment by Cdc42: Key roles for positive feedback and differential mobility. *Small GTPases* **10**, 130–137 (2019).
13. B. Woods *et al*., Parallel actin-independent recycling pathways polarize Cdc42 in budding yeast. *Curr. Biol.* **26**, 2114–2126 (2016).
14. H. Lai *et al*., Temporal regulation of morphogenetic events in Saccharomyces cerevisiae. *Mol. Biol. Cell* **29**, 2069–2083 (2018).
15. D. Pruyne, A. Legesse-Miller, L. Gao, Y. Dong, A. Bretscher, Mechanisms of polarized growth and organelle segregation in yeast. *Annu. Rev. Cell Dev. Biol.* **20**, 559–591 (2004).
16. N. T. Henderson *et al*., Ratiometric GPCR signaling enables directional sensing in yeast. *PLoS Biol.* **17**, e3000484 (2019).
17. X. Wang *et al*., Mating yeast cells use an intrinsic polarity site to assemble a pheromone-gradient tracking machine. *J. Cell Biol.* **218**, 3730–3752 (2019).
18. M. R. Clark-Cotton *et al*., Exploratory polarization facilitates mating partner selection in *Saccharomyces cerevisiae*. *Mol. Biol. Cell* **32**, 1048–1063 (2021).
19. S. A. Ramirez, M. Pablo, S. Burk, D. J. Lew, T. C. Elston, A novel stochastic simulation approach enables exploration of mechanisms for regulating polarity site movement https://doi.org/10.1101/2020.11.30.404657. Deposited 1 December 2020.
20. J. M. Dyer *et al*., Tracking shallow chemical gradients by actin-driven wandering of the polarization site. *Curr. Biol.* **23**, 32–41 (2013).
21. B. Hegemann *et al*., A cellular system for spatial signal decoding in chemical gradients. *Dev. Cell* **35**, 458–470 (2015).
22. G. Vasen, P. Dunayevich, A. Colman-Lerner, Mitotic and pheromone-specific intrinsic polarization cues interfere with gradient sensing in *Saccharomyces cerevisiae*. *Proc. Natl. Acad. Sci. U.S.A.* **117**, 6580–6589 (2020).
23. J. B. Kelley *et al*., RGS proteins and septins cooperate to promote chemotropism by regulating polar cap mobility. *Curr. Biol.* **25**, 275–285 (2015).
24. A. W. McClure *et al*., Role of polarized G protein signaling in tracking pheromone gradients. *Dev. Cell* **35**, 471–482 (2015).
25. D. Ghose, D. Lew, Mechanistic insights into actin-driven polarity site movement in yeast. *Mol. Biol. Cell* **31**, 1085–1102 (2020).
26. B. Hegemann, M. Peter, Local sampling paints a global picture: Local concentration measurements sense direction in complex chemical gradients. *BioEssays* **39**, 1600134 (2017).
27. S. G. Martin, Molecular mechanisms of chemotropism and cell fusion in unicellular fungi. *J. Cell Sci.* **132**, jcs230706 (2019).
28. L. Hicke, H. Riezman, Ubiquitination of a yeast plasma membrane receptor signals its ligand-stimulated endocytosis. *Cell* **84**, 277–287 (1996).
29. L. Hicke, B. Zanolari, H. Riezman, Cytoplasmic tail phosphorylation of the α-factor receptor is required for its ubiquitination and internalization. *J. Cell Biol.* **141**, 349–358 (1998).
30. D. V. Suchkov *et al*., Polarization of the yeast pheromone receptor requires its internalization but not actin-dependent secretion. *Mol. Biol. Cell* **21**, 1737–1752 (2010).
31. K. A. Schandel, D. D. Jenness, Direct evidence for ligand-induced internalization of the yeast alpha-factor pheromone receptor. *Mol. Cell. Biol.* **14**, 7245–7255 (1994).
32. D. D. Jenness, A. C. Burkholder, L. H. Hartwell, Binding of alpha-factor pheromone to Saccharomyces cerevisiae a cells: Dissociation constant and number of binding sites. *Mol. Cell. Biol.* **6**, 318–320 (1986).
33. K. R. Ayscough, D. G. Drubin, A role for the yeast actin cytoskeleton in pheromone receptor clustering and signalling. *Curr. Biol.* **8**, 927–930 (1998).
34. S. Michaelis, STE6, the yeast a-factor transporter. *Semin. Cell Biol.* **4**, 17–27 (1993).
35. N. Valtz, M. Peter, I. Herskowitz, FAR1 is required for oriented polarization of yeast cells in response to mating pheromones. *J. Cell Biol.* **131**, 863–873 (1995).
36. A. Nern, R. A. Arkowitz, A GTP-exchange factor required for cell orientation. *Nature* **391**, 195–198 (1998).
37. A. C. Butty, P. M. Pryciak, L. S. Huang, I. Herskowitz, M. Peter, The role of Far1p in linking the heterotrimeric G protein to polarity establishment proteins during yeast mating. *Science* **282**, 1511–1516 (1998).
38. L. Merlini *et al*., Local pheromone release from dynamic polarity sites underlies cell-cell pairing during yeast mating. *Curr. Biol.* **26**, 1117–1125 (2016).
39. A. S. Howell *et al*., Singularity in polarization: Rewiring yeast cells to make two buds. *Cell* **139**, 731–743 (2009).
40. A. S. Howell *et al*., Negative feedback enhances robustness in the yeast polarity establishment circuit. *Cell* **149**, 322–333 (2012).
41. A. T. Layton *et al*., Modeling vesicle traffic reveals unexpected consequences for Cdc42p-mediated polarity establishment. *Curr. Biol.* **21**, 184–194 (2011).
42. N. S. Savage, A. T. Layton, D. J. Lew, Mechanistic mathematical model of polarity in yeast. *Mol. Biol. Cell* **23**, 1998–2013 (2012).
43. E. Marco, R. Wedlich-Soldner, R. Li, S. J. Altschuler, L. F. Wu, Endocytosis optimizes the dynamic localization of membrane proteins that regulate cortical polarity. *Cell* **129**, 411–422 (2007).
44. S. C. Strickfaden, P. M. Pryciak, Distinct roles for two Galpha-Gbeta interfaces in cell polarity control by a yeast heterotrimeric G protein. *Mol. Biol. Cell* **19**, 181–197 (2008).
45. R. A. Arkowitz, N. Lowe, A small conserved domain in the yeast Spa2p is necessary and sufficient for its polarized localization. *J. Cell Biol.* **138**, 17–36 (1997).
46. A. Nern, R. A. Arkowitz, A Cdc24p-Far1p-Gbetagamma protein complex required for yeast orientation during mating. *J. Cell Biol.* **144**, 1187–1202 (1999).
47. A. Nern, R. A. Arkowitz, G proteins mediate changes in cell shape by stabilizing the axis of polarity. *Mol. Cell* **5**, 853–864 (2000).
48. V. Lakhani, T. C. Elston, Testing the limits of gradient sensing. *PLOS Comput. Biol.* **13**, e1005386 (2017).
49. H. C. Berg, E. M. Purcell, Physics of chemoreception. *Biophys. J.* **20**, 193–219 (1977).
50. R. G. Endres, N. S. Wingreen, Accuracy of direct gradient sensing by cell-surface receptors. *Prog. Biophys. Mol. Biol.* **100**, 33–39 (2009).
51. H. Meinhardt, Orientation of chemotactic cells and growth cones: Models and mechanisms. *J. Cell Sci.* **112**, 2867–2874 (1999).
52. A. W. McClure, K. C. Jacobs, T. R. Zyla, D. J. Lew, Mating in wild yeast: Delayed interest in sex after spore germination. *Mol. Biol. Cell* **29**, 3119–3127 (2018).
53. C. Taxis *et al*., Spore number control and breeding in Saccharomyces cerevisiae: A key role for a self-organizing system. *J. Cell Biol.* **171**, 627–640 (2005).
54. A. Fleißner, S. Herzog, Signal exchange and integration during self-fusion in filamentous fungi. *Semin. Cell Dev. Biol.* **57**, 76–83 (2016).
55. T. C. Südhof, Towards an understanding of synapse formation. *Neuron* **100**, 276–293 (2018).
56. M. Cavey, T. Lecuit, Molecular bases of cell-cell junctions stability and dynamics. *Cold Spring Harb. Perspect. Biol.* **1**, a002998 (2009).
57. L. M. Popescu, M. Gherghiceanu, L. C. Suciu, C. G. Manole, M. E. Hinescu, Telocytes and putative stem cells in the lungs: Electron microscopy, electron tomography and laser scanning microscopy. *Cell Tissue Res.* **345**, 391–403 (2011).
58. J. Rossjohn *et al*., T cell antigen receptor recognition of antigen-presenting molecules. *Annu. Rev. Immunol.* **33**, 169–200 (2015).
59. D. Ghose, K. Jacobs, S. Ramirez. T. Elston, D. Lew, Code and data for "Chemotactic movement of a polarity site enables yeast cells to find their mates." GitHub. https://github.com/DebrajGhose/Chemotactic-polarity-site. Deposited 26 November 2020.